Multiple-source quantitative photoacoustic tomography

Guillaume Bal* Kui Ren†

November 6, 2010

Abstract

Photoacoustic tomography (PAT) is a novel hybrid medical imaging technique that aims to combine the large contrast of optical coefficients with the high resolution capabilities of ultrasounds. We assume that the first step of PAT, namely the reconstruction of a map of absorbed radiation from boundary ultrasound measurement, is done. We focus on quantitative photoacoustic tomography (QPAT), which aims at quantitatively reconstructing optical coefficients from knowledge of the absorbed radiation map.

We present a non-iterative procedure to reconstruct optical coefficients -namely the diffusion and absorption coefficients- and the Grüneisen coefficient in photoacoustic tomography (PAT) when the propagation of radiation is modeled by a second-order elliptic equation. We show that PAT measurements at one given light frequency allow us to unique reconstruct only two out of the above three coefficients even for an arbitrary number of radiation illuminations. We present uniqueness and stability results and demonstrate the accuracy of the reconstruction algorithm on two-dimensional synthetic data.

Key words. Quantitative photoacoustic tomography, inverse problems, interior data, diffusion equation, non-iterative reconstruction, Bregman iteration.

1 Introduction

Photoacoustic tomography (PAT) is a recent *hybrid* medical imaging modality that combines the large contrast of optical parameters with the high resolution capabilities of ultrasonic waves. Optical tomography displays the same large optical contrast but has limited resolution because of multiple scattering [5, 6]. Ultrasounds have much lower contrast because sound speeds display little variations between healthy and unhealthy tissues. However, they theoretically display high resolution capabilities. PAT is based on the photo-acoustic effect, which couples optical and ultrasonic waves. The effect may be described as follows. As

*Department of Applied Physics and Applied Mathematics, Columbia University, New York, NY 10027; gb2030@columbia.edu

†Department of Mathematics, University of Texas at Austin, One University Station C1200, Austin, TX 78712; ren@math.utexas.edu

optical radiation propagates, a fraction of its energy is absorbed and generates thermal expansion of the underlying medium. This mechanical expansion is the source of propagating acoustic signals. Ultrasonic transducers located at the boundary of the domain of interest then record the emitted pressure waves as a function of time.

A first inverse problem in PAT consists of reconstructing the amount of absorbed radiation $H(x)$ from the pressure measurements. For reference to this inverse problem in the physical and engineering literatures, we refer the reader to, e.g., [15, 21, 38, 39] and their references. When the sound speed is constant, explicit formulas have been obtained for a large class of geometries of interest; see [19, 20, 27, 28, 33] and their references. When the sound speed is not constant but known, time reversal algorithms perform well under standard non-trapping conditions as demonstrated in [4, 25, 36]. Note that acoustic absorption is typically neglected in such reconstructions. Accounting for absorption is in fact a difficult and not entirely understood problem [26].

In this paper, we assume that the above first step is done and that $H(x)$ is known. The amount of absorbed radiation $H(x)$ is proportional to the absorption coefficient, $\sigma(x)$, the amount of radiation that reaches a given point $u(x)$, and the Grüneisen coefficient $\Gamma(x)$, which measures how the absorbed radiation is transferred into ultrasounds. The second step of PAT, called quantitative photoacoustics (QPAT), aims to reconstruct the unknown optical parameters and the Grüneisen coefficient from knowledge of $H(x) = \Gamma(x)\sigma(x)u(x)$. For QPAT in the setting of transport equations, we refer the reader to [7]. We consider here the case where radiation propagation is modeled by a second-order elliptic (diffusion) equation. The unknown coefficients are (D, σ, Γ), the diffusion, absorption, and Grüneisen coefficients, respectively.

QPAT may be done in several ways. One methodology is to probe the domain of interest at multiple optical wavelengths (colors) and to reconstruct optical coefficients based on prior information regarding their frequency dependence; see [15, 16], as well as [17] for a different QPAT in the presence of chromophores with intensity-dependent absorption properties. Alternatively, we may use multiple radiation illuminations and acquire as many radiation maps $H(x)$. This is the setting consider in e.g., [10, 35, 40] and in this paper.

In [10], the Grüneisen coefficient is supposed to be known. It is then shown that two well chosen illuminations are sufficient to uniquely and stably reconstruct (D, σ). Moreover, [10] provides an explicit method to solve (D, σ) that relies on solving a *transport equation* and a *second-order elliptic equation*. The well-posedness of the transport equation requires that a vector field constructed from available data satisfy appropriate assumptions. The set of well-chosen illuminations that guaranty such assumptions is not very explicit and is based on the construction of complex geometric optics solutions that depend on the unknown coefficients. The first objectives of this paper is to implement (a modified version of) the reconstruction and show that the reconstruction of (D, σ) is robust for a very large class of illuminations.

The second objective of the paper is to generalize the method in [10] to the reconstruction of (D, σ, Γ). There, we show a somewhat negative result: no matter how many illuminations are used and how many corresponding $H(x)$ are constructed (solving the first inverse wave problem mentioned above), the available data allow us to reconstruct only two functionals of (D, σ, Γ). We show that the two functionals uniquely determine all possible measurements

of the form $H(x) = \Gamma(x)\sigma(x)u(x)$. Finally, we prove that these two functionals uniquely characterize any pair of coefficients in (D, σ, Γ) *provided* that the third one is known. These results are summarized in Theorem 2.2 and Corollary 2.3 below. Section 2 devoted to the presentation of the theoretical results also provides a new stability estimate for the solution to the transport equation. Under the assumption that the vector field in the transport equation does not vanish, we obtain Hölder estimates for the solution to the transport equation in different L^p norms in terms of errors in the measurement $H(x)$ also in L^q norms. These results are summarized in Theorem 2.4 and are based on a direct analysis of the transport equation, as in e.g. [1], rather than on the method of characteristics as in [10].

The practical difficulties inherent to the numerical simulation of the transport and elliptic equations that appear in QPAT are described in section 3. Several numerical experiments presented in section 4 show the robustness of solving the transport and elliptic equations to reconstruct two possibly highly oscillatory coefficients in (D, σ, Γ) from measurements of the form $H(x) = \Gamma(x)\sigma(x)u(x)$. We also show that increasing the number of illuminations allows us to obtain more stable reconstructions of two coefficients when the third one is known. This is consistent with the better stability estimates obtained in [10] in the presence of multiple illuminations.

Let us finally mention that QPAT is one example in the large family of hybrid inverse problems where one aims at reconstructing coefficient from knowledge of internal data. For similar inverse problems with internal data that have been addressed in the mathematical literature, we refer the reader to, e.g., [3, 8, 9, 12, 29, 30, 31, 37].

2 Reconstruction formulas and stability results

In Quantitative photoacoustic tomography (QPAT) in the diffusive regime, photon propagation is modeled by the following second-order elliptic equation

$$\begin{aligned} -\nabla \cdot D(x)\nabla u + \sigma(x)u &= 0 \quad \text{in} \quad X \\ u &= g \quad \text{on} \quad \partial X, \end{aligned} \tag{1}$$

with prescribed Dirichlet conditions at the domain's boundary. Throughout, we will assume that X is a bounded open domain in $\mathbb{R}^d$ with smooth boundary ∂X.

The optical coefficients $(D(x), \sigma(x))$ with $D(x)$ the diffusion coefficient and $\sigma(x)$ the absorption coefficient are assumed to be bounded from above and below by positive constants. In the theoretical analyses below, we also assume that they are Lipschitz continuous, i.e., of class $W^{1,\infty}(X)$.

The information about the coefficients in QPAT takes the following form

$$H(x) = \gamma(x)u(x) \quad \text{a.e. } x \in X, \qquad \text{where } \gamma(x) := \Gamma(x)\sigma(x). \tag{2}$$

The coefficient $\Gamma(x)$ is the Grüneisen coefficient. In many applications in QPAT, it is assumed to be constant. We assume here that it is Lipschitz continuous and bounded above and below by positive constants.

The objective of QPAT is to reconstruct (D, σ, Γ) from knowledge of $H(x)$ in (2) obtained for a given number of illuminations g in (1). The main results of this paper are that:

- Two well chosen illuminations provide two independent relations $\mu(D,\sigma,\Gamma)=\mu$ and $q=q(D,\sigma,\Gamma)$ among the three coefficients (D,σ,Γ) that allow us to uniquely reconstruct two of them provided the third one is known.
- These two independent relations uniquely determine the measurements $H(x)$ for all possible illuminations. In other words, it is impossible to reconstruct the three coefficients (D,σ,Γ) from QPAT data without additional prior information.
- For two well-chosen illuminations, the reconstruction of (μ,q) is Hölder-stable.

Our main assumptions are that:

(i) All coefficients are of class $W^{1,\infty}(X)$ and bounded above and below by positive constants. We assume throughout that the traces of the coefficients (D,σ,Γ) on ∂X are known.

There exist two positive illuminations g_1 and g_2 on ∂X that are the traces of functions of class $C^3(\bar{X})$ and such that the following holds:

(ii) the solutions to (1) are of class $W^{3,p}(X)$ for all $1\leq p<\infty$ by regularity theory and are bounded from below by positive constants by the maximu principle;

(iii) the vector field

$$\beta := H_1\nabla H_2 - H_2\nabla H_1 = H_1^2\nabla\frac{H_2}{H_1} = H_1^2\nabla\frac{u_2}{u_1} = -H_2^2\nabla\frac{H_1}{H_2} \tag{3}$$

is a vector field in $W^{1,\infty}(X)$ (by regularity theory and regularity assumption on γ) and such that

$$|\beta|(x)\geq\alpha_0>0, \qquad \text{a.e. } x\in X. \tag{4}$$

The only real assumption is (4) as the other assumptions are obtained from regularity theory of elliptic equations [23]. The existence of vector fields such that the latter constraint holds is proved in [10]. There, illuminations that are close to traces of specific complex geometric optics (CGO) solutions are shown to be sufficient. For each set of coefficients (D,σ) satisfying (i) above, there is therefore an open set of illuminations for which (4) is guaranteed. However, many vector fields not based on the CGO solutions still satisfy (4).

In dimension $d=2$, a simple condition guarantees that (4) holds. We have the following result [1, 30]:

Lemma 2.1. *Assume that $h=\frac{g_2}{g_1}$ on ∂X is an almost two-to-one function in the sense of [30], i.e., a function that is a two-to-one map except at its minimum and at its maximum (which means that h is strictly monotonic on the two maximal arcs joining the location of its extrema). Then* (4) *is satisfied.*

Proof. Upon multiplying the equation for u_1 by u_2, the equation for u_2 by u_1, and subtracting both relations, we obtain

$$\begin{aligned} -\nabla\cdot(Du_1^2)\nabla\frac{u_2}{u_1} &= 0, \quad \text{in } X \\ \frac{u_2}{u_1} &= \frac{g_2}{g_1}, \quad \text{on } \partial X. \end{aligned} \tag{5}$$

This implies that $v := \frac{u_2}{u_1}$ satisfies an elliptic equation with a diffusion coefficient $\tilde{D} = Du_1^2$ bounded from above and below by positive constants. Note that $\beta = H_1^2 \nabla v$. Results in, e.g., [1, Theorem 1.2] show that ∇v cannot vanish inside X. By the maximum principle and the assumption on h, no critical point of v can occur on ∂X either. This implies that $|\nabla v| > 0$ and that we can find a constant such that (4) holds since H_1^2 is bounded from below by a positive constant and by continuity $|\nabla v|$ attains its (strictly positive) minimum in $\bar{X}$. □

In dimension $d \geq 3$, the above result on the critical points of elliptic solutions no longer holds. However, by continuity, we may verify that (4) is satisfied for a large class of illuminations when D is close to a constant and σ is sufficiently small. For arbitrary coefficients (D, σ) in dimension $d \geq 3$, the only proof that (4) is satisfied for an open set of illuminations is that obtained in [10].

Note also that (4) is a sufficient condition for us to solve the inverse problems of QPAT. In [1], a similar problem is addressed in dimension $d = 2$ without assuming a constraint of the form (4).

Uniqueness result. We first prove a result that provides uniqueness up to a specified transformation.

Theorem 2.2. *Assume that hypotheses (i)-(iii) hold. Then*

(a) $H_1(x)$ and $H_2(x)$ uniquely determine the whole measurement operator $\mathcal{H} : H^{\frac{1}{2}}(\partial X) \to H^1(X)$, which to g defined on ∂X associates $\mathcal{H}(g) = H$ in X defined by (2).

(b) The measurement operator $\mathcal{H}$ uniquely determines the two following functionals of (D, σ, Γ):

$$\mu(x) := \frac{\sqrt{D}}{\Gamma\sigma}(x), \qquad q(x) := -\Big(\frac{\Delta\sqrt{D}}{\sqrt{D}} + \frac{\sigma}{D}\Big)(x). \tag{6}$$

Here Δ is the Laplace operator.

(c) Knowledge of the two functionals μ and q uniquely determines $H_1(x)$ and $H_2(x)$. In other words, the reconstruction of (D, σ, Γ) is unique up to transformations that leave (μ, q) invariant.

Proof. Let us start with (a). As in the derivation of (5), we obtain

$$\begin{aligned} -\nabla \cdot (Du_1^2) \nabla \frac{H_2}{H_1} &= 0, && \text{in } X \\ Du_1^2 &= D_{|\partial X} g_1^2, && \text{on } \partial X. \end{aligned} \tag{7}$$

This is a transport equation in conservative form for Du_1^2. More precisely, this is a transport equation $\nabla \cdot \rho\tilde{\beta} = 0$ for ρ with $\rho_{|\partial X} = 1$ and $\tilde{\beta} = \mu^2\beta = (Du_1^2)\nabla\frac{H_2}{H_1}$. Since $\tilde{\beta} \in W^{1,\infty}(X)$ and is divergence free, the above equation for ρ admits the unique solution $\rho \equiv 1$ owing to the fact that (4) holds. Indeed, we find that $\nabla \cdot (\rho - 1)^2\tilde{\beta} = 0$ by application of the chain rule

with $\rho_{|\partial X} - 1 = 0$ on ∂X. Upon multiplying the equation by $\frac{H_2}{H_1}$ and integrating by parts, we find

$$\int_X (\rho - 1)^2 \mu^2 H_1^2 \Big| \nabla \frac{H_2}{H_1} \Big|^2 dx = 0.$$

Using (4), we deduce that $\rho \equiv 1$. This proves that Du_1^2 is uniquely determined. Dividing by $H_1^2 = (\Gamma\sigma)^2 u_1^2$, this means that $\mu > 0$ is uniquely determined. Note that we do not need the full $W^{1,\infty}(X)$ regularity of β. All we need is that β be sufficiently regular so that the *renormalization property* holds in order to obtain the above integral; see [2, 11, 14, 18]. However, we still need a condition of the form (4) to conclude for the uniqueness to the transport equation. See in particular the treatment of two-dimensional vector fields in [13, 24].

Let now g be an arbitrary boundary condition and let u be the solution to (1) and $H = \mathcal{H}g$ defined by (2). Replacing H_2 above by H yields

$$\begin{aligned} -\nabla \cdot \mu^2 H_1^2 \nabla \frac{H}{H_1} &= 0, && \text{in } X \\ H &= \Gamma_{|\partial X} \sigma_{|\partial X} g, && \text{on } \partial X. \end{aligned} \tag{8}$$

This is a well-defined elliptic equation with a unique solution $H \in H^1(X)$ for $g \in H^{\frac{1}{2}}(\partial X)$. This proves that $\mathcal{H}$ is uniquely determined by (H_1, H_2).

Let us next prove (b). We have already seen that μ was determined by (H_1, H_2), which is clearly determined by $\mathcal{H}$. Moreover, define $v = \sqrt{D}u_1$, which is also uniquely determined based on the results in (a). Define

$$q = \frac{-\Delta v}{v} = -\frac{\Delta(\sqrt{D}u_1)}{\sqrt{D}u_1}.$$

Since u_1 is bounded from below, is sufficiently smooth, and solves (1), a routine calculation shows that q is given by (6).

Finally, we prove (c). Since q is known, we can solve

$$(\Delta + q)v_j = 0, \quad X, \qquad v_j = \sqrt{D_{|\partial X}} g_j \quad \partial X, \qquad j = 1, 2.$$

Because q is of the specific form (6) as a prescribed functional of (D, σ, Γ), it is known that $(\Delta + q)$ does not admit 0 as a (Dirichlet) eigenvalue, for otherwise, 0 would also be a (Dirichlet) eigenvalue of the elliptic operator

$$(-\nabla \cdot D\nabla + \sigma)\cdot = (-\sqrt{D}(\Delta + q)\sqrt{D})\cdot. \tag{9}$$

The latter calculation is the standard Liouville transformation allowing us to replace an elliptic operator by a Schrödinger operator. Thus v_j is uniquely determined for $j = 1, 2$. Now,

$$H_j = \Gamma\sigma u_j = \frac{\Gamma\sigma}{\sqrt{D}} v_j = \frac{v_j}{\mu}, \qquad j = 1, 2,$$

and is therefore uniquely determined by (μ, q). □

On the reconstruction of two coefficients. The above result shows that the unique reconstruction of (D, σ, Γ) is not possible even from knowledge of the full measurement operator $\mathcal{H}$. We therefore face this peculiar situation that two well-chosen illuminations uniquely determine the functionals (μ, q) but that acquiring additional measurements does not provide any new useful information, at least in the absence of any noise in the data. However, if one coefficient in (D, σ, Γ) is known, then the other two are uniquely determined:

Corollary 2.3. *Under the hypotheses of the previous theorem, let* (μ, q) *in* (6) *be known. Then*

(a) If Γ *is known, then* (D, σ) *are uniquely determined.*

(b) If D *is known, then* (σ, Γ) *are uniquely determined.*

(c) If σ *is known, then* (D, Γ) *are uniquely determined.*

Proof. (a) is probably the most practical case as Γ is often assumed to be constant. Since Γ is known, then so is $\Gamma\mu = \sqrt{D}/\sigma$ so that we have the elliptic equation

$$(\Delta + q)\sqrt{D} + \frac{1}{\Gamma\mu} = 0, \quad X, \qquad \sqrt{D}_{|\partial X} = \sqrt{D_{|\partial X}}, \quad \partial X. \tag{10}$$

Again, because of the specific form of q, $(\Delta + q)$ is invertible and the above equation admits a unique solution. Once D is known, then so is σ.

If D is known in (b), then σ is known from q and Γ is known from μ.

Finally in (c), we obtain that from the expression for q that

$$\sqrt{D}(\Delta + q)\sqrt{D} + \sigma = 0 \quad X, \qquad \sqrt{D}_{|\partial X} = \sqrt{D_{|\partial X}}, \quad \partial X. \tag{11}$$

We need to prove a uniqueness results for the above nonlinear equation for $\sqrt{D}$. Let us assume that $\sqrt{D}$ and $\tau\sqrt{D}$ for $0 < \tau$ satisfy the above equation for σ fixed. We have

$$-\sqrt{D}(\Delta + q)\sqrt{D}\tau - \frac{\sigma}{\tau} = 0 \quad X.$$

Thanks to (9), this implies the following equation for τ:

$$-\nabla \cdot D\nabla\tau + \sigma(\tau - \frac{1}{\tau}) = 0, \quad X, \qquad \tau = 1, \quad \partial X.$$

Upon multiplying by $\tau - 1$ and integrating by parts, we find that

$$\int_X D|\nabla(\tau - 1)|^2 dx + \int_X \sigma|\tau - 1|^2 \frac{\tau + 1}{\tau} dx = 0.$$

Since $\tau > 0$, we deduce from the above that $\tau \equiv 1$ so that D is uniquely determined by q. We then retrieve Γ from knowledge of μ. □

Note that the uniqueness results are constructive. All that is required is that we solve a transport equation for μ and then solve an elliptic equation if D is to be reconstructed. These are the steps that will be implemented in the sections on numerical simulations below.

Stability of the solution of the transport equation. Before presenting our numerical framework, we derive a stability result for the reconstruction of μ. A similar result was obtained in [10] by using the stability of the method of characteristics to solve ordinary differential equations. Here, we present a stability result that is directly obtained from the PDE (7) and is quite similar in spirit to estimates obtained in [1] and the notion of renormalization property in transport equation [18].

Theorem 2.4. *We assume that the hypotheses of Theorem 2.2 hold. Let $H = (H_1, H_2)$ be the measurements corresponding to the coefficients (D, σ, Γ) for which hypothesis (iii) holds. Let $\tilde{H} = (\tilde{H}_1, \tilde{H}_2)$ be the measurements corresponding to the same illuminations (g_1, g_2) with another set of coefficients $(\tilde{D}, \tilde{\sigma}, \tilde{\Gamma})$ such that (i) and (ii) still hold. Then we find that*

$$\|\mu - \tilde{\mu}\|_{L^p(X)} \leq C\|H - \tilde{H}\|^{\frac{1}{2}}_{(W^{1,\frac{p}{2}}(X))^2}, \qquad \text{for all } 2 \leq p < \infty. \tag{12}$$

Let us assume, moreover, that $\gamma(x)$ is of class $C^3(\bar{X})$. Then we have the estimate

$$\|\mu - \tilde{\mu}\|_{L^p(X)} \leq C\|H - \tilde{H}\|^{\frac{1}{3}}_{(L^{\frac{p}{2}}(X))^2}, \qquad \text{for all } 2 \leq p < \infty. \tag{13}$$

By interpolation, the latter result implies that

$$\|\mu - \tilde{\mu}\|_{L^\infty(X)} \leq C\|H - \tilde{H}\|^{\frac{p}{3(d+p)}}_{(L^{\frac{p}{2}}(X))^2}, \qquad \text{for all } 2 \leq p < \infty. \tag{14}$$

We may for instance choose $p = 4$ above to measure the noise level in the measurement H in the square integrable norm when noise is described by its power spectrum in the Fourier domain.

Proof. Define $\nu = \mu^2$ and $\tilde{\nu} = \tilde{\mu}^2$ with μ defined in (6) and β and $\tilde{\beta}$ as in (3). Then we find that

$$\nabla \cdot \frac{\nu - \tilde{\nu}}{\nu}(\nu\beta) + \nabla \cdot \tilde{\nu}(\beta - \tilde{\beta}) = 0.$$

Note that $\nu\beta = \mu^2 H_1^2 \nabla \frac{H_2}{H_1}$ is a divergence-free field. Let φ be a twice differentiable, non-negative, function from $\mathbb{R}$ to $\mathbb{R}$ with $\varphi(0) = \varphi'(0) = 0$. Then we find that

$$\nabla \cdot \varphi\Big(\frac{\nu - \tilde{\nu}}{\nu}\Big)(\nu\beta) + \varphi'\Big(\frac{\nu - \tilde{\nu}}{\nu}\Big)\nabla \cdot \tilde{\nu}(\beta - \tilde{\beta}) = 0.$$

Let us multiply this equation by a test function $\zeta \in H^1(X)$ and integrate by parts. Since $\nu = \nu'$ on ∂X, we find

$$\int_X \varphi\Big(\frac{\nu - \tilde{\nu}}{\nu}\Big)\nu\beta \cdot \nabla\zeta dx + \int_X \tilde{\nu}(\beta - \tilde{\beta})\nabla \cdot \Big[\zeta\varphi'\Big(\frac{\nu - \tilde{\nu}}{\nu}\Big)\Big]dx = 0.$$

Upon choosing $\zeta = \frac{H_2}{H_1}$, we find

$$\int_X \varphi\nu H_1^2\Big|\nabla\frac{H_2}{H_1}\Big|^2 dx + \int_X \tilde{\nu}(\beta - \tilde{\beta}) \cdot \nabla\frac{H_2}{H_1}\varphi' dx + \int_X \tilde{\nu}(\beta - \tilde{\beta}) \cdot \nabla\frac{\nu - \tilde{\nu}}{\nu}\frac{H_2}{H_1}\varphi'' dx = 0.$$

Above, φ stands for $\varphi(\frac{\nu-\tilde{\nu}}{\nu})$ in all integrals. By assumption on the coefficients, $\nabla\frac{\nu-\tilde{\nu}}{\nu}$ is bounded a.e.. This is one of our main motivation for assuming that the coefficients are Lipschitz. The middle term is seen to be smaller than the third term and thus we focus on the latter one. Upon taking $\varphi(x) = |x|^p$ for $p \geq 2$ and using assumption (iii), we find that

$$\|\nu - \tilde{\nu}\|^p_{L^p(X)} \leq C \int_X |\beta - \tilde{\beta}||\nu - \tilde{\nu}|^{p-2} dx.$$

By an application of the Hölder inequality, we deduce that

$$\|\nu - \tilde{\nu}\|_{L^p(X)} \leq C\|\beta - \tilde{\beta}\|^{\frac{1}{2}}_{L^{\frac{p}{2}}(X)}.$$

We next write $\beta - \tilde{\beta} = (H_1 - \tilde{H}_1)\nabla H_2 + \tilde{H}_1(\nabla(H_2 - \tilde{H}_2) - \dots$ and use the fact that the solutions to (1) and the coefficients are in $W^{1,\infty}(X)$ to conclude that (12) holds.

The other results are obtained by regularity theory and interpolation. Indeed from regularity results in [23] with coefficients in $W^{1,\infty}(X)$, we find that the solutions to (1) are of class $W^{3,q}(X)$ for all $1 \leq q < \infty$. Since the coefficient γ is of class $C^3(\bar{X})$, then the measurements H_j are of class $W^{3,q}(X)$ for all $1 \leq q < \infty$. Standard Sobolev estimates [23] show that

$$\|H_j - \tilde{H}_j\|_{W^{1,q}(X)} \leq C\|H_j - \tilde{H}_j\|^{\frac{2}{3}}_{L^q(X)}\|H_j - \tilde{H}_j\|^{\frac{1}{3}}_{W^{3,q}(X)}.$$

The last term is bounded by a constant, which gives (13) for $q = \frac{p}{2}$. Another interpolation result states that

$$\|\varphi\|_\infty \leq \|\nabla\varphi\|^\theta_\infty \|\varphi\|^{1-\theta}_p, \qquad \theta = \frac{d}{d+p}.$$

This provides the stability in the uniform norm (14). □

On the reconstruction of one coefficient. We conclude our theoretical section by the reconstruction of one coefficient when the other two coefficients are known. This is significantly simpler than the reconstruction of two coefficients. In none of the cases do we need to solve a transport equation involving the vector field β. The latter was obtained by eliminating σ from the elliptic equation, which is no longer necessary when two coefficients are already known.

When only Γ is unknown, then we solve (1) for u and then construct $\Gamma = \dfrac{H}{\sigma u}$.

When only σ is unknown, then we solve

$$\begin{array}{rcll} -\nabla \cdot D\nabla u(\mathbf{x}) + \dfrac{H}{\Gamma} & = & 0, & \text{in } X \\ u(\mathbf{x}) & = & g(\mathbf{x}), & \text{on } \partial X \end{array}, \qquad \sigma = \frac{H}{\Gamma u}. \tag{15}$$

When only D is unknown, we obtain $u = \frac{H}{\sigma\Gamma}$ and then the above elliptic equation in (15) with $D_{|\partial X}$ known is a transport equation for D. As soon as ∇u is a sufficiently smooth, non-vanishing vector field, then D is uniquely determined by the above linear equation. This problem is analyzed in e.g., [1, 34].

3 Numerical implementation of the reconstruction

In this section and the next, we present a numerical implementation of the reconstruction procedure given in the above theorem and its corollary. We recall that we have to solve a transport equation to reconstruct μ and q and an elliptic equation to reconstruct D when the latter is not known.

All the theoretical results require a certain degree of smoothness of the coefficients we are interested in. The numerical experiments below show that the reconstructions are quite robust even when the coefficients display multiple jump singularities. When this occurs, the numerical implementation has to be done carefully in order to avoid spurious oscillations.

Numerical simulation of the transport equations. The reconstruction procedure we presented above is non-iterative in the sense that we solve the nonlinear inverse problem in one step. There is no iteration on updating the unknowns such as the nonlinear reconstruction schemes in optical tomography [5]. In principle, we only need to solve the transport equation (7) numerically to find $\mu^2 = Du_1^2$. In practice, we have to be careful in the numerical computation because the value the vector field $\beta = H_1^2 \nabla \dfrac{H_2}{H_1}$ usually varies significantly over the domain. We found it numerically useful to normalize the vector field in the transport equation (7). We rewrite the transport equation as

$$\begin{aligned} -\nabla \cdot \big(\mu^2|\beta|\big)\hat{\beta} &= 0 \qquad\qquad \text{in } X \\ \mu^2|\beta| &= \frac{\sqrt{D_{|\partial X}}}{\Gamma_{|\partial X}\sigma_{|\partial X}} \quad \text{on } \partial X, \end{aligned} \tag{16}$$

so that the new vector field $\hat{\beta} = \dfrac{\beta}{|\beta|}$ is a unit vector everywhere.

Regularization in the presence of noise. When the illuminations are chosen so that the vector field β is regular enough, we can solve (16) directly to reconstruct μ (since $|\beta|$ is known). When the data are noisy, the vector field β computed by differentiating $\dfrac{H_2}{H_1}$ may become extremely irregular. Solving the transport equation (16) with such an irregular vector field can be problematic in practice. So we need to regularize the problem. Two ways to regularize it have been considered.

The first way of regularizing the problem is to add a small (controlled by the parameter ε) diffusion term to the transport equation to obtain

$$\begin{aligned} -\varepsilon\Delta\big(\mu^2|\beta|\big) - \nabla \cdot \big(\mu^2|\beta|\big)\hat{\beta} &= 0, \qquad\qquad \text{in } X \\ \mu^2|\beta| &= \frac{\sqrt{D_{|\partial X}}}{\Gamma_{|\partial X}\sigma_{|\partial X}}, \quad \text{on } \partial X. \end{aligned} \tag{17}$$

We then solve this regularized equation to reconstruct μ.

The second way to regularize the problem is to work on the discretized system. We discretize the equation using a first order upwind discontinuous Galerkin method. Let us

denote by $\mathbf{f}$ the discretized version of μ^2, $\mathbf{A}$ the corresponding discretized transport operator and $\mathbf{d}$ the right hand side that come from the boundary condition. We then obtain a system of equations $\mathbf{Af} = \mathbf{d}$. We solve the transport equation in the least-square sense minimizing the following functional

$$\mathcal{O}(\mathbf{f}) = \mathcal{F}(\mathbf{f}) + \mathcal{R}(\mathbf{f}) \equiv \frac{1}{2}\|\mathbf{Af} - \mathbf{d}\|_2^2 + \rho\|\mathbf{f}\|_1. \tag{18}$$

Here we have chosen the regularization term to be the l^1 norm to deal with discontinuous coefficients. To recover smooth coefficients, we should replace the l^1 norm with the l^2 norm, in which case the least-square problem admits the explicit solution $\mathbf{f} = (\mathbf{A}^*\mathbf{A} + \rho\mathbf{I})^{-1}\mathbf{A}^*\mathbf{d}$.

To minimize the objective functional (18) with the l^1 regularization term, we use the Bregman iteration scheme proposed in [32]. The Bregman iteration is characterized by the following iteration, $k \geq 0$, starting with the projection operator $\mathcal{P}_0$:

$$\begin{aligned} \mathbf{f}_{k+1} &= \arg\min_{\mathbf{f}} \mathcal{F}(\mathbf{f}) + \mathcal{R}(\mathbf{f}) - \langle \mathcal{P}_k, \mathbf{f} \rangle \\ \mathcal{P}_{k+1} &= \mathcal{P}_k - \nabla_{\mathbf{f}}\mathcal{F}(\mathbf{f}_{k+1}) \end{aligned} \tag{19}$$

where $\nabla_{\mathbf{f}}\mathcal{F}(\mathbf{f}_{k+1})$ means the evaluation of $\nabla_{\mathbf{f}}\mathcal{F}$ at $\mathbf{f}_{k+1}$. It is proved in [32] that the iteration is well-defined and converges if there are only non-smooth functions in the kernel of $\mathbf{A}$, or at the continuous level, in the kernel of the transport operator with vector field $\hat{\beta}$. For the application of the Bregman method to photoacoustic tomography, we refer to [22].

Setting with multiple illuminations and construction of vector fields. It is shown in [10] that acquiring $2n$ measurements for well-chosen illuminations may improve the stability of the reconstructions. The main idea is that two measurements allow us to obtain $\nabla \cdot \mu^2\beta = 0$ so that $\beta \cdot \nabla\mu^2 + \mu^2\nabla \cdot \beta = 0$ while $2n$ measurements (or sometimes possibly less) allow us to get an equation for the full gradient $\nabla\mu^2$ provided that n linearly independent vector fields can be constructed at each $x \in X$. Instabilities that may appear when solving $\beta \cdot \nabla\mu^2 + \mu^2\nabla \cdot \beta = 0$ in the vicinity of ∂X when β is almost tangent to ∂X no longer appear when we solve a system of the form $\nabla\mu^2 + \Lambda\mu^2 = 0$ with Λ an appropriate known vector.

We have not tried to implement a reconstruction based on solving the above vectorial equation. However, we have demonstrated that acquiring more measurements was unsurprisingly beneficial when noise was present in the data.

In the presence of $I > 2$ data sets, we can write down $I - 1$ transport equations of the form (7) for the same unknown μ but different vector field β_i, $i = 2, ..., I$. We may then solve the over-determined system of $I - 1$ transport equations to reconstruct μ. We can either solve the system in least square sense or solve (16) for different indices and then take the average of the results. We can also use multiple data sets as follows. We divide the data into two groups, H_i, $i = 1, ..., k$ and H_j, $j = k + 1, ..., I$. We then construct the data $\tilde{H}_1 = \sum_{i=1}^{k} H_i$ and $\tilde{H}_2 = \sum_{j=k+1}^{I} H_j$. This is equivalent to saying that $\tilde{H}_1$ and $\tilde{H}_2$ are generated by the illuminations $\tilde{g}_1 = \sum_{i=1}^{k} g_i$ and $\tilde{g}_2 = \sum_{j=k+1}^{I} g_j$, respectively. Numerically, we have observed that both ways of utilizing multiple data sets yielded almost identical reconstruction results.

Elliptic equation with non-smooth diffusion coefficient. The inversion procedure presented in the theoretical section can be applied to the reconstruction of discontinuous diffusion coefficients. Instead of solving (10) for $\sqrt{D}$, we reconstruct non-smooth coefficients D is as follows. We rewrite the diffusion equation, again using the fact that we can reconstruct $v_1 = \sqrt{D}u_1$, and $H_1 = \Gamma\sigma u_1$, as

$$\begin{aligned} -\nabla \cdot v_1^2 \nabla \frac{1}{u_1} &= \frac{H_1}{\Gamma}, \quad \text{in } X, \\ \frac{1}{u_1} &= \frac{1}{g_1}(\mathbf{x}), \quad \text{on } \partial X. \end{aligned} \tag{20}$$

This is an elliptic equation for $\dfrac{1}{u_1}$. In the case when $g_1 > 0$ everywhere on ∂X, (20) provides stable reconstructions of u_1 and thus $\sqrt{D}$, provided that v_1 has been reconstructed faithfully.

4 Simulation results

In all the simulations below, we take the domain of interest to be the square $X = (0, 2)^2$. To simplify notation, we use the notation $\mathbf{x} = (x, y)$ and we will use ∂X_L, ∂X_R, ∂X_T and ∂X_B to denote the left, right, top and bottom parts of the boundary, respectively.

We discretize the diffusion equations, such as (1), (11) and (20), and the transport equations, such as (16) with a first-order discontinuous Galerkin method. The domains are covered with triangular finite element meshes with about 15000 nodes. All the plots are displayed on a structured grid interpolating the quantities defined on the finite element mesh with a MATLAB interpolation algorithm. The semilinear elliptic equation (11) is solved with the standard Newton method. We observed that the Newton iteration converged very rapidly and was very robust with respect to changes in the initial guess.

In all the numerical simulations, we construct the interior data $H(x)$ by solving the diffusion equation with the true coefficients on an extremely fine finite element mesh, evaluating $\Gamma\sigma u$ on the fine mesh, and interpolating it onto the coarser mesh used in the reconstructions. The data constructed this way thus contain some "noise" due to the mesh difference and interpolation, Nonetheless, we will refer to these data as the "noise-free" data. We estimated that the "noise" level was less than 0.2%.

A simple noise model. We will also perform reconstructions using noisy data. For want of a more physically realistic noise model, here we simply add a discrete (on the coarse mesh) i.i.d. noise to the data set $H(\mathbf{x})$ in the following sense

$$\tilde{H}(\mathbf{x}) = H(\mathbf{x}) * (1 + \alpha \text{random}(\mathbf{x})), \tag{21}$$

where random($\mathbf{x}$) is an uncorrelated random field taking values in $[-1, 1]$ and α controls the noise level. Such a noise is sufficient to generate highly oscillatory vector fields that complicate the simulation of the transport equation. When sufficiently noisy data are acquired, we need to run a de-noising process on the vector field, which we chose as a low-pass

filter constructed by a 5-point sliding averaging process. Although this may not be the best denoising process available, it worked quite well numerically to remove the high-frequency noise generated in (21). A more systematic study of noise in QPAT, including low-frequency noise that is much harder to handle, still needs to be done.

We will measure the quality of the reconstruction using the relative L^2 error between reconstructed and true coefficients. We will use $\mathcal{E}_\sigma^C$ and $\mathcal{E}_\sigma^N$ to denote the relative L^2 error in the reconstruction of σ using "clean" and "noisy" data respectively. All noisy data are with 8% random noise constructed as in (21).

Vector fields with different illumination patterns. We show here that many pairs of illuminations can generate a vector field that can connect every point inside the domain with a point on the boundary of the domain.

Experiment 1. In the first numerical experiment, we plot the vector fields generated from different pair of illuminations for a problem with the following discontinuous absorption and diffusion coefficients:

$$\sigma(\mathbf{x}) = \begin{cases} 0.3, & \mathbf{x} \in X_1 \\ 0.1, & \mathbf{x} \in X \backslash X_1 \end{cases} \qquad D(\mathbf{x}) = \begin{cases} 0.04, & \mathbf{x} \in X_2 \cup X_3 \\ 0.02, & \mathbf{x} \in \mathbf{x} \in X \backslash (X_2 \cup X_3). \end{cases}$$

where the inclusions are $X_1 = [0.3\ 0.7] \times [0.3\ 0.7]$, $X_2 = [0.8\ 1.2] \times [1.3\ 1.7]$ and $X_3 = [1.3\ 1.7] \times [0.3\ 1.1]$. The Grüneisen coefficient is taken to be constant and equals 0.5 although it does not play a role in the plot of the vector field. We consider four different pairs of illuminations (g_1, g_2), (g_3, g_4), (g_5, g_6) and (g_7, g_8) that are defined respectively as follows.

$$g_1 = \begin{cases} 1.0, & \mathbf{x} \in \partial X_T \cup \partial X_L, \\ 0.5, & \mathbf{x} \in \partial X_B \cup \partial X_R \end{cases} \qquad g_2 = \begin{cases} 0.5, & \mathbf{x} \in \partial X_T \cup \partial X_L, \\ 1.0, & \mathbf{x} \in \partial X_B \cup \partial X_R \end{cases}$$

$$g_3 = \begin{cases} 1.0, & \mathbf{x} \in \partial X_T \cup \partial X_L, \\ 0.0, & \mathbf{x} \in \partial X_B \cup \partial X_R \end{cases} \qquad g_4 = \begin{cases} 0.0, & \mathbf{x} \in \partial X_T \cup \partial X_L, \\ 1.0, & \mathbf{x} \in \partial X_B \cup \partial X_R \end{cases}$$

$$g_5 = \begin{cases} 1.0, & \mathbf{x} \in \partial X_L, \\ 0.0, & \mathbf{x} \in \partial X_R \end{cases} \qquad g_6 = \begin{cases} 0.0, & \mathbf{x} \in \partial X_L, \\ 1.0, & \mathbf{x} \in \partial X_R \end{cases}$$

$$g_7 = \begin{cases} x, & \mathbf{x} \in \partial X_T, \\ y, & \mathbf{x} \in \partial X_L, \\ 0.0, & \mathbf{x} \in \partial X_B \cup \partial X_R \end{cases} \qquad g_8 = \begin{cases} 0.0, & \mathbf{x} \in \partial X_T \cup \partial X_L, \\ x, & \mathbf{x} \in \partial X_B, \\ y, & \mathbf{x} \in \partial X_R \end{cases}$$

The results of the numerical experiment is shown in Fig. 1. Even though slight errors occur near boundaries in a couple of cases, in general the constructed vector fields are quite accurate. Note that for better visualization purpose, we have plotted the vector field on a mesh that is 8 times coarser than the mesh used in the numerical reconstructions shown below.

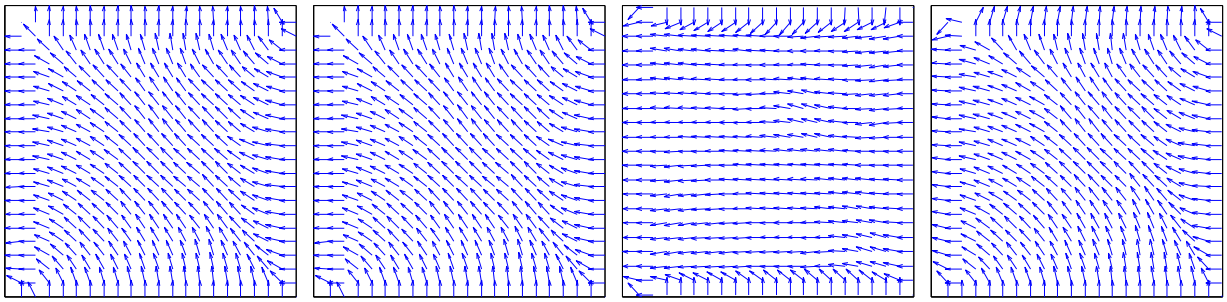

Figure 1: Normalized vector fields constructed in Experiment 1. The illumination pairs used are $(g_1,\ g_2)$, $(g_3,\ g_4)$, $(g_5,\ g_6)$ and $(g_7,\ g_8)$ from left to right.

Numerical simulations with smooth coefficients. We now present some reconstructions of smooth coefficients. We present in Experiments 2, 3 and 4 the reconstructions of $(\Gamma,\, \sigma)$, $(\Gamma,\, D)$, and $(\sigma,\, D)$ respectively.

Experiment 2. In this experiment, we intend to reconstruct the Grüneisen and absorption coefficient:

$$\Gamma(\mathbf{x}) = 0.8 + 0.4\tanh(4x-4)) \quad \text{and} \quad \sigma(\mathbf{x}) = 0.1 + 0.2e^{-(x-1)^2-(y-1)^2}.$$

The diffusion coefficient is a known constant $D(\mathbf{x}) = 0.02$. The measurements are constructed with the two sources g_1 and g_2. The results of the numerical experiment are shown in Fig. 2. The relative L^2 errors in the reconstructions are $\mathcal{E}_\Gamma^C = 0.2\%$, $\mathcal{E}_\Gamma^N = 1.1\%$, $\mathcal{E}_\sigma^C = 0.2\%$ and $\mathcal{E}_\sigma^N = 1.6\%$.

Experiment 3. In this experiment, we intend to reconstruct the Grüneisen and diffusion coefficients:

$$\Gamma(\mathbf{x}) = 0.6 + 0.3\sin(\pi x) \quad \text{and} \quad D(\mathbf{x}) = 0.03 + 0.01\sin(\pi y).$$

The absorption coefficient is the known constant $\sigma = 0.1$. The measurements are again constructed with the two sources g_1 and g_2. The results of the numerical experiment are shown in Fig. 3. The relative L^2 errors in the reconstructions are $\mathcal{E}_\Gamma^C = 0.2\%$, $\mathcal{E}_\Gamma^N = 1.1\%$, $\mathcal{E}_D^C = 0.2\%$ and $\mathcal{E}_D^N = 1.4\%$.

Experiment 4. In this experiment, the absorption and diffusion coefficients are given by

$$\sigma(\mathbf{x}) = 0.1 + 0.2e^{-(x-1)^2-(y-1)^2} \quad \text{and} \quad D(\mathbf{x}) = 0.03 + 0.02\sin(\pi x)\sin(\pi y),$$

respectively. The Grüneisen coefficient $\Gamma = 0.5$. The measurements are constructed with the two sources g_1 and g_2 described above. The results of the numerical experiment are shown in Fig. 4. The relative L^2 errors are $\mathcal{E}_\sigma^C = 0.2\%$, $\mathcal{E}_\sigma^N = 0.8\%$, $\mathcal{E}_D^C = 0.1\%$ and $\mathcal{E}_D^N = 3.1\%$.

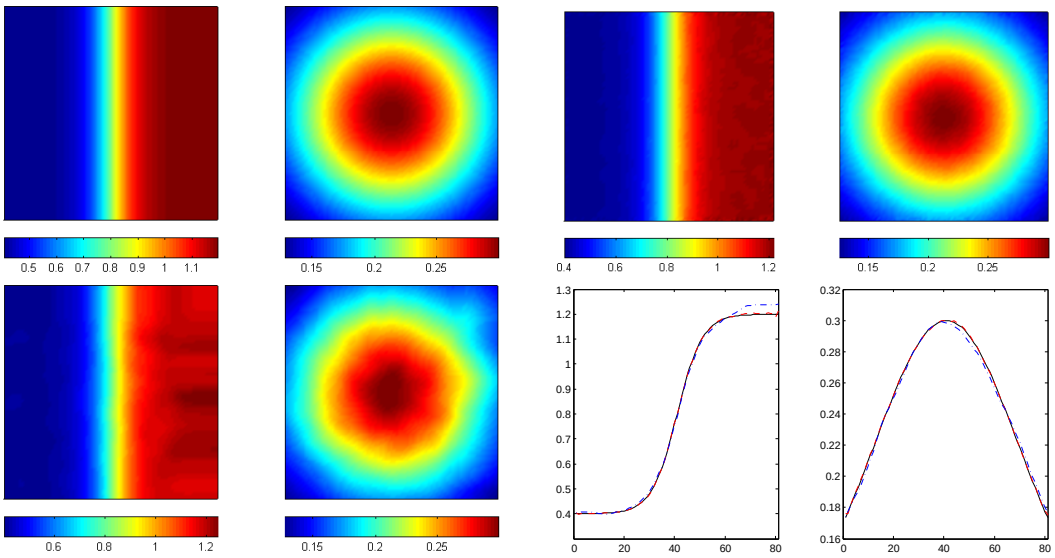

Figure 2: Experiment 2. From top left to bottom right are: true Γ and σ, reconstructed Γ and σ with noise-free data, reconstructed Γ and σ with noisy data, cross-section of true (solid) and reconstructed (red dashed and blue dot-dashed) Γ and σ along $y = 1$ with noisy data.

Numerical simulations with discontinuous coefficients. We now consider the reconstruction of discontinuous Grüneisen, absorption and diffusion coefficients. The reconstructions are done with the Bregman iteration method that was described above. As we have seen, the discontinuities in $\Gamma(\mathbf{x})$ and $\sigma(\mathbf{x})$ cause no problem in the reconstructions, while the discontinuities in the diffusion coefficient require special treatment.

Experiment 5. In this experiment, we intend to reconstruct the Grüneisen coefficient that contains three inclusions at $X_1 = [0.3\ 0.7] \times [0.3\ 0.7]$, $X_2 = [0.8\ 1.2] \times [1.3\ 1.7]$ and $X_3 = [1.3\ 1.7] \times [0.3\ 1.1]$ and a smooth absorption coefficient:

$$\Gamma(\mathbf{x}) = \begin{cases} 0.8, & \mathbf{x} \in X_1 \cup X_2 \\ 0.4, & \mathbf{x} \in X \backslash (X_1 \cup X_2) \end{cases} \quad \text{and} \quad \sigma(\mathbf{x}) = \begin{cases} 0.3, & \mathbf{x} \in X_3 \\ 0.1, & \mathbf{x} \in X \backslash X_3. \end{cases}$$

The diffusion coefficient is a known constant $D(\mathbf{x}) = 0.02$. The measurements are constructed with the same sources as in Experiment 1. The results of the numerical experiment are shown in Fig. 5. The relative L^2 errors in the reconstructions are $\mathcal{E}_\Gamma^C = 0.2\%$, $\mathcal{E}_\Gamma^N = 5.0\%$, $\mathcal{E}_\sigma^C = 0.2\%$ and $\mathcal{E}_\sigma^N = 10.7\%$.

Experiment 6. In this experiment, we intend to reconstruct the discontinuous Grüneisen and diffusion coefficients:

$$\Gamma(\mathbf{x}) = \begin{cases} 0.3, & \mathbf{x} \in X_1 \\ 0.1, & \mathbf{x} \in X \backslash X_1 \end{cases} \quad \text{and} \quad D(\mathbf{x}) = \begin{cases} 0.04, & \mathbf{x} \in X_2 \cup X_3 \\ 0.02, & \mathbf{x} \in \mathbf{x} \in X \backslash (X_2 \cup X_3) \end{cases}$$

The absorption coefficient is a known constant $\sigma(\mathbf{x}) = 0.1$. The measurements are constructed with the same two sources g_1 and g_2 as in the previous cases. The results of the

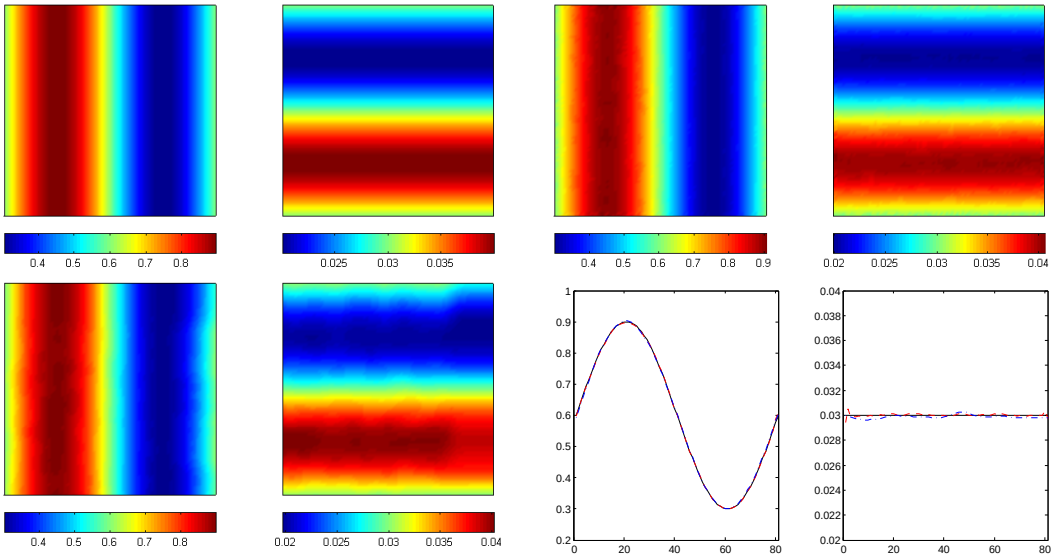

Figure 3: Experiment 3. From top left to bottom right are: true Γ and D, reconstructed Γ and D with noise-free data, reconstructed Γ and D with noisy data, cross-section of true (solid) and reconstructed (red dashed and blue dot-dashed) Γ and D along $y = 1$ with noisy data.

numerical experiment are shown in Fig. 6. The relative L^2 errors in the reconstructions are $\mathcal{E}_\sigma^C = 0.2\%$, $\mathcal{E}_\sigma^N = 6.2\%$, $\mathcal{E}_D^C = 0.2\%$ and $\mathcal{E}_D^N = 7.1\%$.

Experiment 7. In this experiment, we intend to reconstruct the absorption coefficient

$$\sigma(\mathbf{x}) = \begin{cases} 0.1 + 0.1 * (\text{sign}(\text{random}) + 1), & \mathbf{x} \in X_{ij},\ 1 \le i, j \le 10 \\ 0.1, & \mathbf{x} \in \mathbf{x} \in X \backslash (\cup X_{i,j}) \end{cases}$$

where random is a random number in $[-1\ 1]$ and X_{ij} is the box $X_{ij} = [0.3 + 0.1(i-1)\ \ 0.3 + 0.1i] \times [0.3 + 0.1(j-1)\ \ 0.3 + 0.1j]$, and the discontinuous diffusion coefficient

$$D(\mathbf{x}) = \begin{cases} 0.02 + 0.02 * (\text{sign}(\text{random}) + 1), & \mathbf{x} \in X_{ij},\ 1 \le i, j \le 10 \\ 0.02, & \mathbf{x} \in \mathbf{x} \in X \backslash (\cup X_{i,j}) \end{cases}$$

where X_{ij} is the box $X_{ij} = [0.7 + 0.1(i-1)\ \ 0.7 + 0.1i] \times [0.7 + 0.1(j-1)\ \ 0.7 + 0.1j]$. The Grüneisen coefficient is a known constant $\Gamma(\mathbf{x}) = 0.5$. The measurements are constructed with the two sources g_1 and g_2. One realization of the coefficients and the results of the numerical experiment are shown in Fig. 7. The relative L^2 error in the reconstructions are $\mathcal{E}_\sigma^C = 0.2\%$, $\mathcal{E}_\sigma^N = 13.0\%$, $\mathcal{E}_D^C = 0.2\%$ and $\mathcal{E}_D^N = 16.2\%$.

Numerical simulations with multiple illuminations. We have seen that multiple illuminations would not provide extra information that would allow us to reconstruct all three coefficients. However, more acquiring more data indeed improves the reconstruction by averaging out noise in the data.

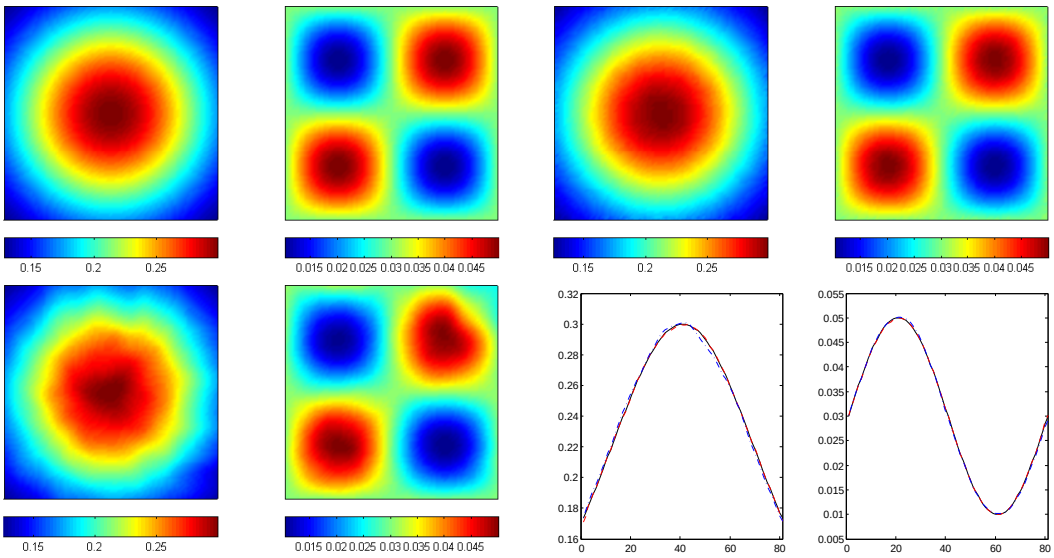

Figure 4: Experiment 4. From top left to bottom right are: true σ and D, reconstructed σ and D with noise-free data, reconstructed σ and D with noisy data, cross-section of true (solid) and reconstructed (red dashed and blue dot-dashed) σ and D along $y = 0.5$ with noisy data.

Experiment 8. We present here a reconstruction of the absorption and diffusion coefficients in Experiment 6 with multiple data sets. We have a total of 10 measurements constructed using the sources g_1-g_{10}, with g_1 - g_8 given above and g_9, g_10 given as

$$g_9 = \begin{cases} \dfrac{e^{-\frac{(y-1)^2}{2\ 0.1^2}}}{\sqrt{2\pi 0.1^2}}, & \mathbf{x} \in \partial\Omega_L, \\ 0.0, & \mathbf{x} \in \partial\Omega \backslash \partial\Omega_L \end{cases} \qquad g_{10} = \begin{cases} \dfrac{e^{-\frac{(y-1)^2}{2\ 0.1^2}}}{\sqrt{2\pi 0.1^2}}, & \mathbf{x} \in \partial\Omega_R, \\ 0.0, & \mathbf{x} \in \partial\Omega \backslash \partial\Omega_R \end{cases}$$

The data are polluted with again 8% of random noise. The transport equations are solved in the least square sense with L_1 sparsity regularization using the Bregman iteration method. The reconstruction results are presented in Fig. 8. The relative L^2 error in the reconstructions are $E_\sigma^C = 0.1\%$, $E_\sigma^N = 9.3\%$, $E_D^C = 0.1\%$ and $E_D^N = 9.6\%$. The reconstruction in the case of noisy data is indeed improved.

Acknowledgment

GB was supported in part by NSF Grants DMS-0554097 and DMS-0804696. KR was supported in part by NSF Grant DMS-0914825.

References

[1] G. Alessandrini, *An identification problem for an elliptic equation in two variables*, Ann. Mat. Pura Appl., 145 (1986), pp. 265–296.

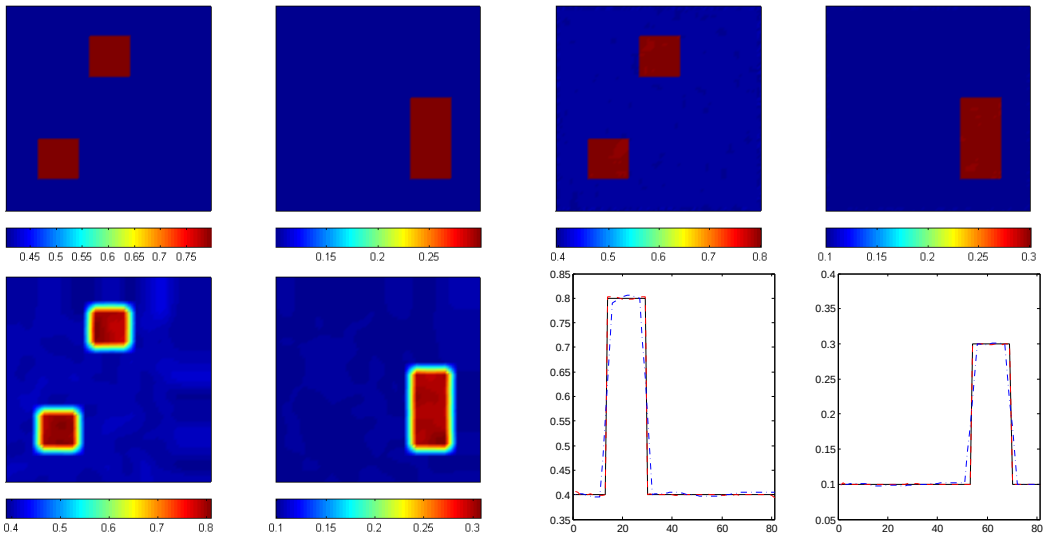

Figure 5: Experiment 5. From top left to bottom right are: true Γ and σ, reconstructed Γ and σ with noise-free data, reconstructed Γ and σ with noisy data, cross-section of true (solid) and reconstructed (red dashed and blue dot-dashed) Γ and σ along $y = 0.5$ with noisy data.

[2] L. Ambrosio, *Transport equation and Cauchy problem for BV vector fields*, Invent. Math., 158 (2004), p. 227260.

[3] H. Ammari, E. Bonnetier, Y. Capdeboscq, M. Tanter, and M. Fink, *Electrical impedance tomography by elastic deformation*, SIAM J. Appl. Math., 68 (2008), pp. 1557–1573.

[4] H. Ammari, E. Bossy, V. Jugnon, and H. Kang, *Mathematical models in photoacoustic imaging of small absorbers*, SIAM Review, (2010).

[5] S. R. Arridge and J. C. Schotland, *Optical tomography: forward and inverse problems*, Inverse Problems, 25 (2010), p. 123010.

[6] G. Bal, *Inverse transport theory and applications*, Inverse Problems, 25 (2009), p. 053001.

[7] G. Bal, A. Jollivet, and V. Jugnon, *Inverse transport theory of Photoacoustics*, Inverse Problems, 26 (2010), p. 025011.

[8] G. Bal, K. Ren, G. Uhlmann, and T. Zhou, *Quantitative thermo-acoustics and related problems*, submitted.

[9] G. Bal and J. C. Schotland, *Inverse Scattering and Acousto-Optics Imaging*, Phys. Rev. Letters, 104 (2010), p. 043902.

[10] G. Bal and G. Uhlmann, *Inverse diffusion theory for photoacoustics*, Inverse Problems, 26(8) (2010), p. 085010.

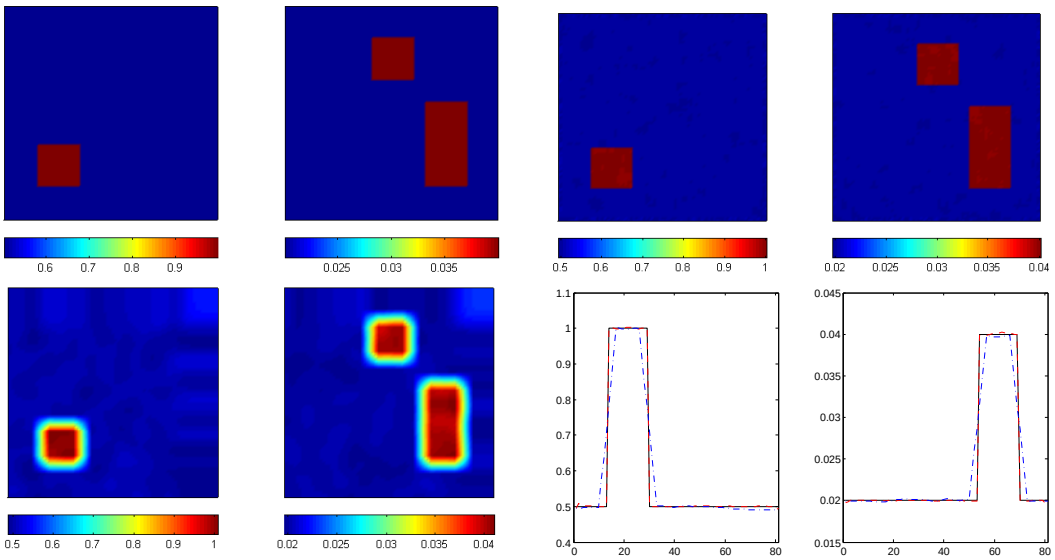

Figure 6: Experiment 6. From top left to bottom right are: true Γ and D, reconstructed Γ and D with noise-free data, reconstructed Γ and D with noisy data, cross-section of true (solid) and reconstructed (red dashed and blue dot-dashed) Γ and D along $y = 1$.

[11] F. Bouchut and G. Crippa, *Uniqueness, renormalization and smooth approximations for linear transport equations*, SIAM J. Math. Anal., 38 (2006), pp. 1316–1328.

[12] Y. Capdeboscq, J. Fehrenbach, F. de Gournay, and O. Kavian, *Imaging by modification: numerical reconstruction of local conductivities from corresponding power density measurements*, SIAM J. Imaging Sciences, 2 (2009), pp. 1003–1030.

[13] F. Colombini, G. Crippa, and J. Rauch, *A note on two-dimensional transport with bounded divergence*, Comm. Partial Differential Equations, 31 (2006), pp. 1109–1115.

[14] F. Colombini and N. Lerner, *Uniqueness of continuous solutions for BV vector fields*, Duke Math. J., 111 (2002), p. 357384.

[15] B. T. Cox, S. R. Arridge, and P. C. Beard, *Estimating chromophore distributions from multiwavelength photoacoustic images*, J. Opt. Soc. Am. A, 26 (2009), pp. 443–455.

[16] B. T. Cox, J. G. Laufer, and P. C. Beard, *The challenges for quantitative photoacoustic imaging*, Proc. of SPIE, 7177 (2009), p. 717713.

[17] ——, *Quantitative photoacoustic image reconstruction using fluence dependent chromophores*, Biomedical Optics Express, 1(1) (2010), pp. 201–208.

[18] R. J. DiPerna and P.-L. Lions, *On the cauchy problem for boltzmann equations: global existence and weak stability*, Ann. of Math. (2), 130 (1989), pp. 321–366.

[19] D. Finch and Rakesh., *Recovering a function from its spherical mean values in two and three dimensions*, in Photoacoustic imaging and spectroscopy L. H. Wang (Editor), CRC Press, (2009).

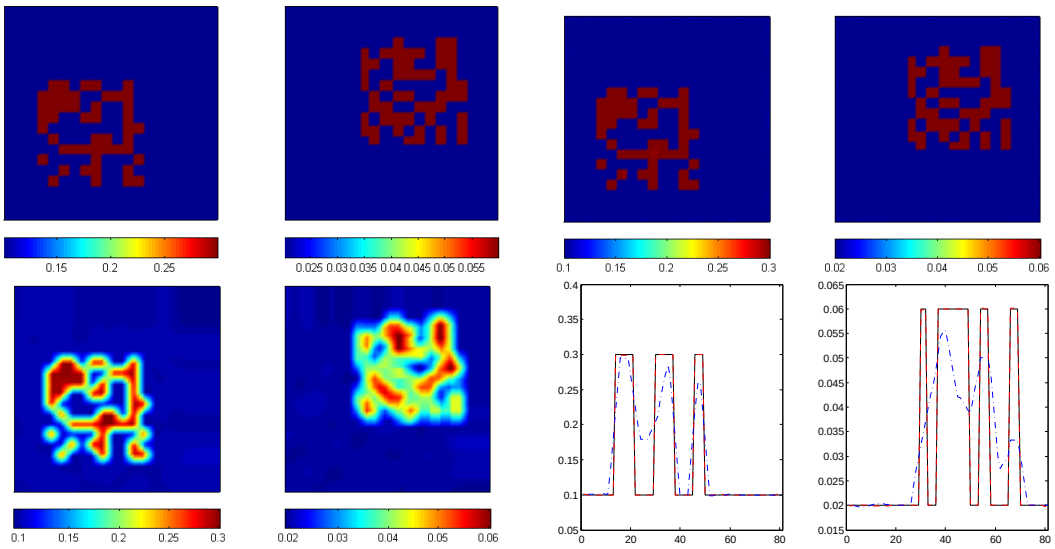

Figure 7: Experiment 7. From top left to bottom right are: true σ and D, reconstructed σ and D with noise-free data, reconstructed σ and D with noisy data, cross-section of true (solid) and reconstructed (red dashed and blue dot-dashed) σ and D along $y = 1$ with noisy data.

[20] S. K. Finch, D. Patch and Rakesh., *Determining a function from its mean values over a family of spheres*, SIAM J. Math. Anal., 35 (2004), pp. 1213–1240.

[21] A. R. Fisher, A. J. Schissler, and J. C. Schotland, *Photoacoustic effect for multiply scattered light*, Phys. Rev. E, 76 (2007), p. 036604.

[22] H. Gao, H. Zhao, and S. Osher, *Bregman methods in quantitative photoacoustic tomography*. CAM Report 10-42, UCLA, 2010.

[23] D. Gilbarg and N. S. Trudinger, *Elliptic Partial Differential Equations of Second Order*, Springer-Verlag, Berlin, 1977.

[24] M. Hauray, *On two-dimensional Hamiltonian transport equations with L^p_{loc} coefficients*, Ann. IHP. Anal. Non Lin., 20 (2003), p. 625644.

[25] Y. Hristova, P. Kuchment, and L. Nguyen, *Reconstruction and time reversal in thermoacoustic tomography in acoustically homogeneous and inhomogeneous media*, Inverse Problems, 24 (2008), p. 055006.

[26] R. Kowar and O. Scherzer, *Photoacoustic imaging taking into account attenuation*, in Mathematics and Algorithms in Tomography, vol. 18, Mathematisches Forschungsinstitut Oberwolfach, 2010, pp. 54–56.

[27] P. Kuchment and L. Kunyansky, *Mathematics of thermoacoustic tomography*, Euro. J. Appl. Math., 19 (2008), pp. 191–224.

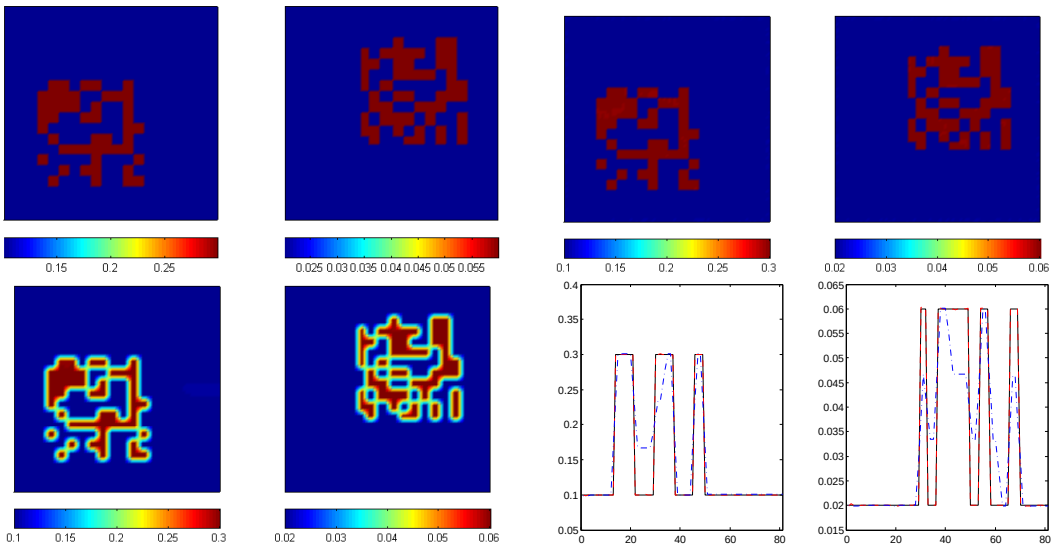

Figure 8: Experiment 8. From top left to bottom right are: true σ and D, reconstructed σ and D with noise-free data, reconstructed σ and D with noisy data, cross-section of true (solid) and reconstructed (red dashed and blue dot-dashed) σ and D along $y = 1$.

[28] L. A. Kunyansky, *Explicit inversion formulae for the spherical mean radon transform*, Inverse Problems, 23 (2007), pp. 373–383.

[29] J. R. McLaughlin and J. Yoon, *Unique identifiability of elastic parameters from time-dependent interior displacement measurement*, Inverse Problems, 20 (2004), p. 2545.

[30] A. Nachman, A. Tamasan, and A. Timonov, *Conductivity imaging with a single measurement of boundary and interior data*, Inverse Problems, 23 (2007), pp. 2551–2563.

[31] A. Nachman, A. Tamasan, and A. Timonov, *Recovering the conductivity from a single measurement of interior data*, Inverse Problems, 25 (2009), p. 035014.

[32] S. Osher, M. Burger, D. Goldfarb, J. Xu, and W. Yin, *An iterative regularization method for total variation based image restoration*, Multiscale Model. Simul., 4 (2005), pp. 460–489.

[33] S. Patch and O. Scherzer, *Photo- and thermo- acoustic imaging*, Inverse Problems, 23 (2007), pp. S1–10.

[34] G. R. Richter, *An Inverse Problem for the Steady State Diffusion Equation*, SIAM J. Applied Math., 41 (1981), pp. 210–221.

[35] J. Ripoll and V. Ntziachristos, *Quantitative point source photoacoustic inversion formulas for scattering and absorbing medium*, Phys. Rev. E, 71 (2005), p. 031912.

[36] P. Stefanov and G. Uhlmann, *Thermoacoustic tomography with variable sound speed*, Inverse Problems, 25 (2009), p. 075011.

[37] F. Triki, *Uniqueness and stability for the inverse medium problem with internal data*, Inverse Problems, 26 (2010), p. 095014.

[38] L. V. Wang, *Ultrasound-mediated biophotonic imaging: a review of acousto-optical tomography and photo-acoustic tomography*, Journal of Disease Markers, 19 (2004), pp. 123–138.

[39] M. Xu and L. V. Wang, *Photoacoustic imaging in biomedicine*, Rev. Sci. Instr., 77 (2006), p. 041101.

[40] R. J. Zemp, *Quantitative photoacoustic tomography with multiple optical sources*, Applied Optics, 49 (2010), pp. 3566–3572.